AIMS Mathematics, 11(8): 26359–26396.
DOI: 10.3934/math.20261058
Received: 06 April 2026
Revised: 02 August 2026
Accepted: 18 August 2026
Published: 24 August 2026

https://www.aimspress.com/journal/Math

Research article

Cost-effective strategies for controlling date palm mite infestations: an optimal control approach

Saleh Fahad Aljurbua[1,*] **and Moustafa El-Shahed**[1,2]

[1] Department of Mathematics, College of Science, Qassim University, Saudi Arabia

[2] Department of Computer Science, College of Engineering and Information Technology, Onaizah Colleges, Qassim 56447, Saudi Arabia

* **Correspondence:** Email: s.aljurbua@qu.edu.sa.

Abstract: This paper develops and analyzes a stage-structured mathematical model for the population dynamics of date palm mite infestations, incorporating density-dependent saturation in egg production and explicitly accounting for the egg, larval, nymphal, and adult stages. A population reproduction threshold is derived to characterize the transition between the pest's extinction and persistence. Stability analysis shows that the extinction equilibrium is locally and globally asymptotically stable when the reproduction threshold remains below unity. Conversely, when this threshold exceeds one, a unique positive coexistence equilibrium emerges. The model is further shown to undergo a forward bifurcation at the critical threshold, indicating a smooth transition from extinction to persistence. The global stability of the coexistence equilibrium is established using persistence theory and the Li–Muldowney geometric approach. In addition, a sensitivity analysis identifies the key biological parameters governing the long-term dynamics of the mite population. An optimal control framework is formulated to minimize the infestation while balancing the implementation costs of mechanical, biological, and chemical interventions. The necessary optimality conditions are derived using Pontryagin's maximum mrinciple. Numerical simulations support the theoretical findings, and the subsequent cost-effectiveness analysis identifies the most economically efficient control strategy. Overall, the proposed framework provides useful insights into the development of sustainable and cost-effective integrated pest management strategies for date palm protection.

Keywords: mathematical model; optimization problems; sensitivity analysis; Lyapunov function; date palm mite
Mathematics Subject Classification: 92D25, 49J15, 49K15, 93C95, 92D40

1. Introduction

Date palm (*Phoenix dactylifera* L.) is one of the most important fruit crops in arid and semi-arid regions, where it plays a vital role in food security, rural livelihoods, and sustainable agricultural development. The economic value of date production has increased considerably in recent years owing to the growing global demand for high-quality dates. Nevertheless, date palm cultivation remains highly vulnerable to pest infestations that can substantially reduce both fruit yield and market quality [1]. Among these pests, the date palm mite *Oligonychus afrasiaticus* (McGregor) (Acari: Tetranychidae) is recognized as one of the most destructive species. It attacks fruits during their developmental stages, causing discoloration, dehydration, and premature fruit drop, thereby leading to significant economic losses [2, 3]. The biology of *O. afrasiaticus* is characterized by a sequence of distinct developmental stages consisting of eggs, larvae, nymphs, and adults [4, 5]. Adult mites are solely responsible for reproduction, whereas the immature stages contribute to the overall population dynamics through their sequential development toward the reproductive adult stage. Moreover, increasing population density intensifies competition for food resources and suitable oviposition sites, resulting in a reduction in the effective reproduction rate. These biological features indicate that a stage-structured mathematical description is more suitable than an unstructured population model for representing the dynamics of date palm mite infestations [6–8].

Mathematical models have become indispensable tools for understanding the dynamics of biological populations and for predicting their long-term behavior under different ecological and management scenarios [9–11]. In pest management, such models provide a quantitative framework for evaluating the effects of biological processes and intervention strategies before their implementation in the field. Stage-structured models are particularly attractive because they explicitly describe the transitions between successive developmental stages, thereby providing a biologically realistic representation of the life cycle of insects and mites [12]. Furthermore, incorporating density-dependent mechanisms into these models enables a more realistic description of population regulation resulting from resource limitation and intraspecific competition.

Various management strategies have been proposed to suppress date palm mite populations. Mechanical control mainly targets the early developmental stages through the removal of infested plant material, biological control relies on natural enemies to suppress the mobile stages of the mite, whereas chemical control increases mortality across multiple developmental stages. These interventions differ substantially in their biological effectiveness, implementation costs, and environmental impacts. Consequently, identifying economically efficient combinations of these strategies has become an important objective of integrated pest management [13]. Optimal control theory provides a rigorous mathematical framework for determining time-dependent intervention policies that balance pest suppression against implementation costs. Instead of prescribing fixed control levels, optimal control identifies intervention schedules that minimize the overall infestation while accounting for the economic cost of control measures. When combined with cost-effectiveness analysis, this approach allows different management strategies to be compared not only in terms of their biological performance but also with respect to their economic efficiency, thereby providing practical guidance for decision- makers [14, 15].

Although mathematical models have been widely applied to insect and mite population dynamics, relatively few studies have focused specifically on stage-structured models for the date palm mite.

Existing studies mainly emphasize biological observations or numerical simulations, while rigorous analytical investigations of the underlying dynamical system remain rather limited. In particular, the threshold behavior governing the mites' extinction and persistence, the global dynamics of the coexistence equilibrium, the role of density-dependent recruitment, and the economic evaluation of different control strategies have received comparatively little attention. To the best of our knowledge, no previous study has integrated stage-structured population modeling, qualitative dynamical analysis, uniform persistence, optimal control, and cost-effectiveness analysis within a unified framework for *O. afrasiaticus*. Motivated by these observations, this paper develops a new stage-structured mathematical model describing the population dynamics of the date palm mite. The model incorporates a Beverton–Holt density-dependent recruitment function that captures the reduction in reproductive success caused by competition for limited resources while preserving biological feasibility. The qualitative analysis establishes the positivity, boundedness, existence of equilibria, population reproduction threshold, local stability, uniform persistence, and global asymptotic stability of the coexistence equilibrium using the Li–Muldowney geometric approach. In addition, forward bifurcation and sensitivity analyses are performed to investigate the influence of the model's parameters on the population dynamics. Finally, an optimal control problem involving mechanical, biological, and chemical interventions is formulated, and the resulting strategies are assessed using cost-effectiveness analysis to identify economically efficient pest management policies.

The remainder of this paper is organized as follows. Section 2 presents the mathematical model together with the underlying biological assumptions. Section 3 investigates the qualitative properties of the model, including the existence and stability of equilibria, persistence, and global dynamics. Section 4 presents numerical simulations together with sensitivity analysis. Section 5 develops the optimal control formulation and evaluates the proposed intervention strategies through cost-effectiveness analysis. Finally, Section 6 summarizes the main findings and discusses their biological implications.

2. Model formulation

To describe the population dynamics of the date palm mite *O. afrasiaticus* during the summer season, we develop a stage-structured mathematical model based on the four principal developmental stages of its life cycle, namely eggs, larvae, nymphs, and adults. Let $E(t)$, $L(t)$, $N(t)$, and $A(t)$ denote the population densities of eggs, larvae, nymphs, and adults, respectively, at time t. Experimental observations indicate that the complete life cycle of *O. afrasiaticus* during the summer season lasts approximately 12 days. Consequently, the developmental transition rates between successive stages are assumed to remain constant over the time interval considered. Adult mites constitute the only reproductive stage of the life cycle, whereas the immature stages develop sequentially until reaching adulthood. Under natural conditions, egg production is limited by the availability of food resources, space, and suitable oviposition sites. As the population density increases, competition among individuals gradually reduces the effective oviposition rate. To represent this biological mechanism while maintaining a non-negative recruitment rate, we adopt a Beverton–Holt-type density-dependent recruitment function [16–18] rather than the classical logistic recruitment term. This formulation captures the gradual saturation of egg production under crowding conditions while ensuring that the recruitment rate remains positive and bounded for all biologically feasible population densities. The

model is based on the following biological assumptions.

- The mite population is divided into four developmental stages: eggs (E), larvae (L), nymphs (N), and adults (A).
- Adult mites produce eggs at the per-capita oviposition rate β.
- Egg production is regulated by density-dependent competition. This mechanism is represented by the recruitment function

$$\frac{\beta A}{1 + \dfrac{A + N + L}{K}},$$

  where $K > 0$ denotes the saturation constant controlling the strength of density dependence. When the population density is low, the recruitment rate is approximately proportional to the adult population. As the densities of larvae, nymphs, and adults increase, competition for limited resources progressively reduces the effective oviposition rate, causing the recruitment rate to approach a finite saturation level.
- Eggs develop into larvae at a rate γ_E, larvae develop into nymphs at a rate γ_L, and nymphs develop into adults at a rate γ_N.
- The parameters μ_E, μ_L, μ_N, and μ_A denote the natural mortality rates of eggs, larvae, nymphs, and adults, respectively.

Figure 1 presents a schematic representation of the proposed stage-structured model. The diagram illustrates the developmental transitions, the Beverton–Holt-type density-dependent recruitment process, and the natural mortality associated with each developmental stage. Mortality may result from several biological factors, including predation, pathogenic infections, and environmental stress.

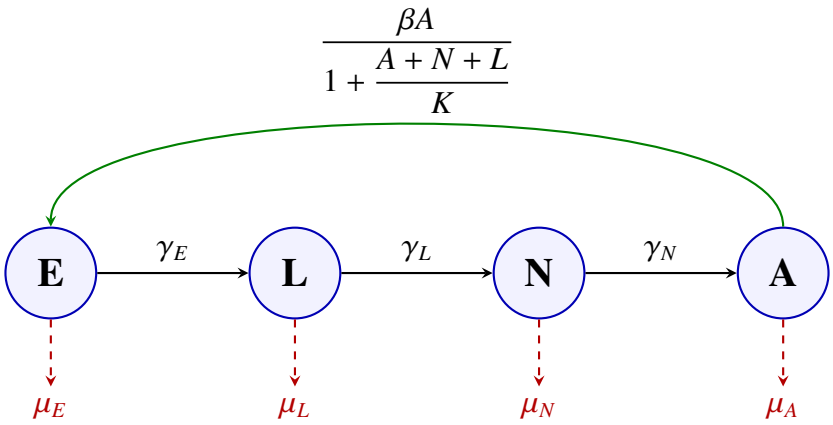

Figure 1. Stage-structured model of the date palm mite population, illustrating density-dependent Beverton–Holt recruitment, developmental transitions, and natural mortality.

Based on the biological assumptions above, the population dynamics of the date palm mite are governed by the following system of nonlinear ordinary differential equations:

$$\begin{cases} \dfrac{dE}{dt} = \dfrac{\beta A}{1 + \dfrac{A+N+L}{K}} - (\gamma_E + \mu_E)E, \\ \dfrac{dL}{dt} = \gamma_E E - (\gamma_L + \mu_L)L, \\ \dfrac{dN}{dt} = \gamma_L L - (\gamma_N + \mu_N)N, \\ \dfrac{dA}{dt} = \gamma_N N - \mu_A A. \end{cases} \tag{1}$$

The first equation describes density-dependent egg production together with egg development and natural mortality. The remaining equations represent the successive developmental transitions and natural mortality of the larval, nymphal, and adult stages.

Remark 1. *The Beverton–Holt-type recruitment function remains positive and bounded for all non-negative population densities. Consequently, the model preserves biological feasibility while accounting for the density-dependent reduction in egg production caused by competition for limited resources.*

The model is supplemented with the non-negative initial conditions

$$(E(0), L(0), N(0), A(0)) = (E_0, L_0, N_0, A_0) \in \mathbb{R}^4_+.$$

Model parameters

The biological parameters together with their numerical values are summarized in Table 1. Unless otherwise stated, the parameter values are taken from the experimental demographic study of Ben Chaaban et al. [19].

Table 1. Biological parameters used in the model [19].

Parameter	Description	Value
β	Oviposition rate (eggs per female per day)	1.5
γ_E	Egg-to-larva transition rate	0.161
γ_L	Larva-to-nymph transition rate	0.404
γ_N	Nymph-to-adult transition rate	0.352
μ_E	Egg mortality rate	0.056
μ_L	Larval mortality rate	0.021
μ_N	Nymphal mortality rate	0.039
μ_A	Adult mortality rate	0.075
K	Saturation constant for density-dependent oviposition	100

For the convenience of the reader, the principal mathematical symbols used throughout this paper are summarized in Table 2. Unless otherwise stated, all state variables are assumed to be non-negative.

Table 2. Notation used throughout the paper.

Symbol	Description
$E(t)$	Egg population density
$L(t)$	Larval population density
$N(t)$	Nymph population density
$A(t)$	Adult population density
$\mathcal{R}_0$	Population reproduction threshold
P_0	Extinction equilibrium
P^*	Coexistence equilibrium
Ω_M	Compact positively invariant absorbing set
Ω_*	Interior compact positively invariant set
$u_1(t)$	Mechanical control variable
$u_2(t)$	Biological control variable
$u_3(t)$	Chemical control variable
Q^*	Total equilibrium infestation burden
T_a	Total averted weighted infestation burden
T_c	Total intervention cost
ACER	Average cost-effectiveness ratio
ICER	Incremental cost-effectiveness ratio

3. Mathematical analysis

In this section, we investigate the fundamental qualitative properties of System (1). We first establish that the model is mathematically well posed and biologically meaningful by proving the existence, uniqueness, positivity, and boundedness of the solutions. We then identify a positively invariant absorbing region, which serves as the biologically feasible state space for the subsequent qualitative analysis.

3.1. Well-posedness, positivity, and boundedness

Theorem 2. *For every initial condition*

$$(E(0), L(0), N(0), A(0)) = (E_0, L_0, N_0, A_0) \in \mathbb{R}^4_+,$$

System (1) *admits a unique local solution defined on a maximal interval* $[0, t_{\max})$. *Moreover, the nonnegative orthant* $\mathbb{R}^4_+$ *is positively invariant.*

Proof. The vector field associated with System (1) is continuously differentiable on an open neighborhood of $\mathbb{R}^4_+$. Consequently, it is locally Lipschitz continuous. The Picard–Lindelöf theorem therefore guarantees the existence and uniqueness of a local solution on a maximal interval [20]. $[0, t_{\max})$.

To establish positivity, we verify that the vector field is quasipositive on the boundary of the nonnegative orthant.

At $E = 0$, we have

$$\left.\frac{dE}{dt}\right|_{E=0} = \frac{\beta A}{1 + \dfrac{A + N + L}{K}} \geq 0.$$

Similarly,

$$\left.\frac{dL}{dt}\right|_{L=0} = \gamma_E E \geq 0,$$

$$\left.\frac{dN}{dt}\right|_{N=0} = \gamma_L L \geq 0,$$

and

$$\left.\frac{dA}{dt}\right|_{A=0} = \gamma_N N \geq 0.$$

Hence, the vector field points inward (or is tangent) on every boundary face of $\mathbb{R}^4_+$. Therefore, no component of a solution starting in $\mathbb{R}^4_+$ can become negative, and the nonnegative orthant is positively invariant. □

Having established positivity, we next derive an a priori estimate showing that the total mite population remains bounded.

Lemma 3. *Every solution of System* (1) *with the initial data in* $\mathbb{R}^4_+$ *is bounded on its interval of existence and is uniformly ultimately bounded.*

Proof. Define

$$S(t) = E(t) + L(t) + N(t) + A(t),$$

and

$$S_1(t) = L(t) + N(t) + A(t).$$

Summing the equations of System (1) gives

$$\dot{S} = \frac{\beta A}{1 + \dfrac{S_1}{K}} - \mu_E E - \mu_L L - \mu_N N - \mu_A A.$$

Let

$$\mu = \min\{\mu_E, \mu_L, \mu_N, \mu_A\} > 0.$$

Since

$$0 \leq A \leq S_1,$$

it follows that

$$\frac{A}{1+\frac{S_1}{K}} \leq \frac{S_1}{1+\frac{S_1}{K}} = \frac{KS_1}{K+S_1} \leq K.$$

Therefore, we have

$$\dot{S} \leq \beta K - \mu S.$$

Applying the comparison principle yields

$$S(t) \leq S(0)e^{-\mu t} + \frac{\beta K}{\mu}\left(1 - e^{-\mu t}\right), \qquad 0 \leq t < t_{\max}.$$

Consequently,

$$S(t) \leq \max\left\{S(0), \frac{\beta K}{\mu}\right\},$$

and

$$\limsup_{t\to\infty} S(t) \leq \frac{\beta K}{\mu}.$$

Hence, every solution is bounded on its interval of existence and is uniformly ultimately bounded. □

The preceding estimate rules out finite-time blow-up of the local solution and therefore allows it to be continued globally.

Corollary 4. *For every initial condition in $\mathbb{R}^4_+$, System* (1) *admits a unique nonnegative solution defined for all $t \geq 0$.*

Proof. By Theorem 2, a unique local solution exists on a maximal interval $[0, t_{\max})$. Lemma 3 shows that the solution remains bounded on this interval. Since the vector field is locally Lipschitz continuous, finite-time blow-up cannot occur. Therefore, the standard continuation theorem for ordinary differential equations [21] implies that $t_{\max} = \infty$. □

We now identify a biologically feasible region in which the long-term dynamics of the system will be investigated.

Corollary 5. *For every*

$$M > \frac{\beta K}{\mu},$$

the set

$$\Omega_M = \left\{(E, L, N, A) \in \mathbb{R}^4_+ : E + L + N + A \leq M\right\}$$

is a compact positively invariant absorbing set for System (1).

Proof. Since Ω_M is closed and bounded in $\mathbb{R}^4$, it is compact.

On the boundary

$$S = M.$$

Lemma 3 gives

$$\dot{S} \leq \beta K - \mu M < 0.$$

Hence, the vector field points strictly inward on the boundary of Ω_M, which proves the positive invariance.

Moreover

$$\limsup_{t\to\infty} S(t) \leq \frac{\beta K}{\mu} < M.$$

Therefore, every solution starting in $\mathbb{R}^4_+$ eventually enters Ω_M and remains there. Thus, Ω_M is an absorbing set. □

Remark 6. *The positively invariant absorbing set Ω_M constitutes the biologically feasible region of the model. All subsequent analyses, including the existence and stability of equilibria, persistence, bifurcation, and optimal control, are carried out within this feasible region.*

3.2. The population reproduction threshold $\mathcal{R}_0$

To analyze the threshold dynamics of System (1), we derive the population reproduction threshold $\mathcal{R}_0$ using the next-generation matrix method [22, 23]. Let $x = (E, L, N, A)^T$. Following the next-generation framework, the vector $\mathcal{F}(x)$ contains the rates at which newly produced individuals enter the egg compartment, whereas $\mathcal{V}(x)$ contains all the transition and removal terms.

Since new individuals enter the population through egg production by adult mites, we define

$$\mathcal{F}(x) = \begin{pmatrix} \dfrac{\beta A}{1 + \dfrac{A+N+L}{K}} \\ 0 \\ 0 \\ 0 \end{pmatrix}, \qquad \mathcal{V}(x) = \begin{pmatrix} (\gamma_E + \mu_E)E \\ (\gamma_L + \mu_L)L - \gamma_E E \\ (\gamma_N + \mu_N)N - \gamma_L L \\ \mu_A A - \gamma_N N \end{pmatrix}.$$

The Jacobian matrices of $\mathcal{F}$ and $\mathcal{V}$, evaluated at the extinction equilibrium $P_0 = (0, 0, 0, 0)$, are

$$F = D\mathcal{F}(P_0) = \begin{pmatrix} 0 & 0 & 0 & \beta \\ 0 & 0 & 0 & 0 \\ 0 & 0 & 0 & 0 \\ 0 & 0 & 0 & 0 \end{pmatrix}, \qquad V = D\mathcal{V}(P_0) = \begin{pmatrix} \gamma_E + \mu_E & 0 & 0 & 0 \\ -\gamma_E & \gamma_L + \mu_L & 0 & 0 \\ 0 & -\gamma_L & \gamma_N + \mu_N & 0 \\ 0 & 0 & -\gamma_N & \mu_A \end{pmatrix}.$$

A direct calculation gives

$$\mathcal{R}_0 = \rho(FV^{-1}) = \frac{\beta\gamma_E\gamma_L\gamma_N}{(\gamma_E + \mu_E)(\gamma_L + \mu_L)(\gamma_N + \mu_N)\mu_A}.$$

Biologically, $\mathcal{R}_0$ represents the expected number of adult female mites produced by a single adult female during her average lifetime when the mite population is initially rare. It can be written as

$$\mathcal{R}_0 = \beta\left(\frac{\gamma_E}{\gamma_E + \mu_E}\right)\left(\frac{\gamma_L}{\gamma_L + \mu_L}\right)\left(\frac{\gamma_N}{\gamma_N + \mu_N}\right)\frac{1}{\mu_A}.$$

Here, β/μ_A represents the expected number of eggs produced during the average adult lifetime, whereas the three fractions represent the probabilities of surviving the egg, larval, and nymphal stages, respectively.

3.3. Equilibrium points

The system admits the extinction equilibrium

$$P_0 = (0, 0, 0, 0).$$

To determine the positive coexistence equilibrium

$$P^* = (E^*, L^*, N^*, A^*),$$

we set the right-hand sides of System (1) equal to zero. Let

$$\alpha_1 = \gamma_E + \mu_E, \qquad \alpha_2 = \gamma_L + \mu_L, \qquad \alpha_3 = \gamma_N + \mu_N.$$

From the last three equilibrium equations, we obtain

$$E^* = C_E A^*, \qquad L^* = C_L A^*, \qquad N^* = C_N A^*,$$

where

$$C_E = \frac{\mu_A \alpha_2 \alpha_3}{\gamma_E \gamma_L \gamma_N}, \qquad C_L = \frac{\mu_A \alpha_3}{\gamma_L \gamma_N}, \qquad C_N = \frac{\mu_A}{\gamma_N}.$$

Substituting these relations into the first equation of System (1) for $A^* > 0$ yields

$$\frac{\beta}{1 + \dfrac{A^*(1 + C_L + C_N)}{K}} = \alpha_1 C_E.$$

Recalling the basic reproduction number $\mathcal{R}_0 = \frac{\beta}{\alpha_1 C_E}$, we solve for A^* to obtain

$$A^* = \frac{K(\mathcal{R}_0 - 1)}{1 + C_L + C_N}.$$

Consequently, the coexistence equilibrium can be explicitly expressed as

$$P^* = \left(C_E A^*,\, C_L A^*,\, C_N A^*,\, A^*\right),$$

which exists uniquely in the positive octant $\mathbb{R}^4_{++}$ if and only if $\mathcal{R}_0 > 1$.

3.4. Local stability of the extinction equilibrium

Theorem 7. *The extinction equilibrium P_0 is locally asymptotically stable if $\mathcal{R}_0 < 1$ and unstable if $\mathcal{R}_0 > 1$.*

Proof. The Jacobian matrix of System (1) at P_0 is

$$J(P_0) = \begin{pmatrix} -\alpha_1 & 0 & 0 & \beta \\ \gamma_E & -\alpha_2 & 0 & 0 \\ 0 & \gamma_L & -\alpha_3 & 0 \\ 0 & 0 & \gamma_N & -\mu_A \end{pmatrix}.$$

The characteristic polynomial of $J(P_0)$ is

$$p(\lambda) = \lambda^4 + g_1\lambda^3 + g_2\lambda^2 + g_3\lambda + g_4,$$

where

$$\begin{aligned} g_1 &= \alpha_1 + \alpha_2 + \alpha_3 + \mu_A, \\ g_2 &= \alpha_3\mu_A + \alpha_2(\alpha_3 + \mu_A) + \alpha_1(\alpha_2 + \alpha_3 + \mu_A), \\ g_3 &= \alpha_2\alpha_3\mu_A + \alpha_1\left[\alpha_3\mu_A + \alpha_2(\alpha_3 + \mu_A)\right], \\ g_4 &= \alpha_1\alpha_2\alpha_3\mu_A - \beta\gamma_E\gamma_L\gamma_N \\ &= \alpha_1\alpha_2\alpha_3\mu_A(1 - \mathcal{R}_0). \end{aligned}$$

Clearly, $g_1, g_2, g_3 > 0$. If $\mathcal{R}_0 < 1$, then $g_4 > 0$. Moreover, the second Hurwitz determinant is

$$\Delta_2 = g_1g_2 - g_3,$$

and direct simplification gives

$$\Delta_2 = \alpha_1^2(\alpha_2 + \alpha_3 + \mu_A) + \alpha_1(\alpha_2 + \alpha_3 + \mu_A)^2 + (\alpha_2 + \alpha_3)(\alpha_2 + \mu_A)(\alpha_3 + \mu_A) > 0.$$

The third Hurwitz determinant is

$$\Delta_3 = g_3(g_1g_2 - g_3) - g_1^2g_4.$$

After algebraic simplification, it can be expressed as

$$\begin{aligned} \Delta_3 = {} & (\alpha_2 + \alpha_3)\alpha_1^3(\alpha_2 + \mu_A)(\alpha_3 + \mu_A) + \alpha_2^3\alpha_3\mu_A(\alpha_3 + \mu_A) \\ & + \alpha_1^2\Big[(\alpha_2 + \alpha_3)(\alpha_2 + \mu_A)(\alpha_3 + \mu_A)(\alpha_2 + \alpha_3 + \mu_A) + \beta\gamma_E\gamma_L\gamma_N\Big] \\ & + \alpha_1\Big[\alpha_2^3(\alpha_3 + \mu_A)^2 + \alpha_2^2(\alpha_3 + \mu_A)(\alpha_3^2 + 3\alpha_3\mu_A + \mu_A^2) \\ & \quad + 2\alpha_2\left(\alpha_3\mu_A(\alpha_3 + \mu_A)^2 + \beta\gamma_E\gamma_L\gamma_N\right) \\ & \quad + (\alpha_3 + \mu_A)\left(\alpha_3^2\mu_A^2 + 2\beta\gamma_E\gamma_L\gamma_N\right)\Big] \\ & + \beta\gamma_E\gamma_L\gamma_N(\alpha_3 + \mu_A)^2 \\ & + \alpha_2(\alpha_3 + \mu_A)\left(\alpha_3^2\mu_A^2 + 2\beta\gamma_E\gamma_L\gamma_N\right) \end{aligned}$$

$$+ \alpha_2^2 \left(\alpha_3 \mu_A (\alpha_3 + \mu_A)^2 + \beta \gamma_E \gamma_L \gamma_N \right).$$

Since all model parameters are positive, every term in the expression above is positive, and hence $\Delta_3 > 0$. Therefore, when $\mathcal{R}_0 < 1$, all the Routh–Hurwitz conditions are satisfied, and all eigenvalues of $J(P_0)$ have negative real parts. Thus, P_0 is locally asymptotically stable.

If $\mathcal{R}_0 > 1$, then $g_4 < 0$. Since

$$p(0) = g_4 < 0 \qquad \text{and} \qquad p(\lambda) \longrightarrow +\infty \quad \text{as } \lambda \longrightarrow +\infty,$$

the intermediate value theorem implies that p has at least one positive real root. Consequently, P_0 is unstable when $\mathcal{R}_0 > 1$. □

The following theorem provides a sufficient condition for the global stability of the extinction equilibrium point.

3.5. Global stability of the extinction equilibrium

Theorem 8. *If $\mathcal{R}_0 < 1$, then the extinction equilibrium P_0 is globally asymptotically stable in $\mathbb{R}^4_+$.*

Proof. Consider the Lyapunov function

$$V(E, L, N, A) = c_1 E + c_2 L + c_3 N + A,$$

where

$$c_1 = \frac{\gamma_E \gamma_L \gamma_N}{\alpha_1 \alpha_2 \alpha_3}, \qquad c_2 = \frac{\gamma_L \gamma_N}{\alpha_2 \alpha_3}, \qquad c_3 = \frac{\gamma_N}{\alpha_3}.$$

Since $c_1, c_2, c_3 > 0$, the function V is positive definite on $\mathbb{R}^4_+$; namely,

$$V(E, L, N, A) \geq 0,$$

with equality if and only if

$$(E, L, N, A) = P_0.$$

Differentiating V along the solutions of System (1) gives

$$\begin{aligned} \dot{V} &= c_1 \dot{E} + c_2 \dot{L} + c_3 \dot{N} + \dot{A} \\ &= c_1 \frac{\beta A}{1 + \dfrac{A + N + L}{K}} + (-c_1 \alpha_1 + c_2 \gamma_E) E \\ &\quad + (-c_2 \alpha_2 + c_3 \gamma_L) L + (-c_3 \alpha_3 + \gamma_N) N - \mu_A A. \end{aligned}$$

By the choice of the constants c_1, c_2, c_3, we have

$$-c_1 \alpha_1 + c_2 \gamma_E = -c_2 \alpha_2 + c_3 \gamma_L = -c_3 \alpha_3 + \gamma_N = 0.$$

Hence,

$$\dot{V} = \frac{c_1 \beta A}{1 + \dfrac{A + N + L}{K}} - \mu_A A.$$

Since

$$1 + \frac{A + N + L}{K} \geq 1,$$

it follows that

$$\dot{V} \leq (c_1\beta - \mu_A)A.$$

Moreover,

$$c_1\beta = \frac{\beta\gamma_E\gamma_L\gamma_N}{\alpha_1\alpha_2\alpha_3} = \mu_A\mathcal{R}_0.$$

Therefore,

$$\dot{V} \leq \mu_A(\mathcal{R}_0 - 1)A.$$

Since $\mathcal{R}_0 < 1$, we have

$$\mu_A(\mathcal{R}_0 - 1) < 0,$$

and hence

$$\dot{V} \leq 0 \qquad \text{for all } (E, L, N, A) \in \mathbb{R}^4_+.$$

It remains to determine the largest invariant subset of

$$\mathcal{Z} = \left\{(E, L, N, A) \in \mathbb{R}^4_+ : \dot{V} = 0\right\}.$$

Since

$$\mu_A(\mathcal{R}_0 - 1) < 0,$$

the equality

$$\dot{V} = 0$$

can only occur when

$$A = 0.$$

Along an invariant trajectory contained in $\mathcal{Z}$, the fourth equation of System (1) becomes

$$\dot{A} = \gamma_N N.$$

Hence, the invariance of the condition $A = 0$ requires

$$N = 0.$$

Similarly,

$$\dot{N} = \gamma_L L,$$

implies

$$L = 0,$$

and finally,

$$\dot{L} = \gamma_E E,$$

implies

$$E = 0.$$

Therefore,

$$E = L = N = A = 0,$$

and consequently the largest invariant subset of $\mathcal{Z}$ is

$$\{P_0\}.$$

By the positivity and boundedness results established previously, every solution starting in $\mathbb{R}^4_+$ remains non-negative and eventually enters a compact positively invariant set. Therefore, LaSalle's invariance principle yields

$$\lim_{t\to\infty}(E(t), L(t), N(t), A(t)) = P_0.$$

Hence, the extinction equilibrium P_0 is globally asymptotically stable in $\mathbb{R}^4_+$. □

3.6. Stability of the coexistence equilibrium

The following theorem provides a sufficient condition for the local asymptotic stability of the coexistence equilibrium.

3.7. Local stability of the coexistence equilibrium

Theorem 9. *Assume that $\mathcal{R}_0 > 1$ so that the coexistence equilibrium P^* exists. If*

$$\Delta_3 = \eta_1\eta_2\eta_3 - \eta_3^2 - \eta_1^2\eta_4 > 0,$$

then P^* is locally asymptotically stable.

Proof. Let

$$q = 1 + \frac{A + N + L}{K}.$$

The Jacobian matrix of System (1) is

$$J(E, L, N, A) = \begin{pmatrix} -\alpha_1 & -\dfrac{\beta A}{Kq^2} & -\dfrac{\beta A}{Kq^2} & \dfrac{\beta}{q} - \dfrac{\beta A}{Kq^2} \\ \gamma_E & -\alpha_2 & 0 & 0 \\ 0 & \gamma_L & -\alpha_3 & 0 \\ 0 & 0 & \gamma_N & -\mu_A \end{pmatrix}.$$

At the coexistence equilibrium,

$$q^* = 1 + \frac{A^* + N^* + L^*}{K} = \mathcal{R}_0.$$

Define

$$b = \frac{\beta A^*}{K\mathcal{R}_0^2}, \qquad d = \frac{\beta}{\mathcal{R}_0} - b.$$

Then

$$J(P^*) = \begin{pmatrix} -\alpha_1 & -b & -b & d \\ \gamma_E & -\alpha_2 & 0 & 0 \\ 0 & \gamma_L & -\alpha_3 & 0 \\ 0 & 0 & \gamma_N & -\mu_A \end{pmatrix}.$$

The characteristic polynomial of $J(P^*)$ is

$$\lambda^4 + \eta_1\lambda^3 + \eta_2\lambda^2 + \eta_3\lambda + \eta_4 = 0,$$

where

$$\begin{aligned}
\eta_1 &= \alpha_1 + \alpha_2 + \alpha_3 + \mu_A,\\
\eta_2 &= \alpha_1\alpha_2 + \alpha_1\alpha_3 + \alpha_1\mu_A + \alpha_2\alpha_3 + \alpha_2\mu_A + \alpha_3\mu_A + b\gamma_E,\\
\eta_3 &= \alpha_1\alpha_2\alpha_3 + \mu_A\,(\alpha_1\alpha_2 + \alpha_1\alpha_3 + \alpha_2\alpha_3) + b\gamma_E(\alpha_3 + \mu_A + \gamma_L),\\
\eta_4 &= \alpha_1\alpha_2\alpha_3\mu_A + b\gamma_E\mu_A(\alpha_3 + \gamma_L) - d\gamma_E\gamma_L\gamma_N.
\end{aligned}$$

Since

$$d = \frac{\beta}{\mathcal{R}_0} - b$$

and

$$\frac{\beta\gamma_E\gamma_L\gamma_N}{\mathcal{R}_0} = \alpha_1\alpha_2\alpha_3\mu_A,$$

the constant coefficient simplifies to

$$\eta_4 = b\gamma_E\left[\gamma_L\gamma_N + \mu_A(\alpha_3 + \gamma_L)\right] > 0.$$

Thus,

$$\eta_i > 0, \qquad i = 1, 2, 3, 4.$$

By the Liénard–Chipart criterion, the coexistence equilibrium is locally asymptotically stable provided that

$$\Delta_3 = \eta_1\eta_2\eta_3 - \eta_3^2 - \eta_1^2\eta_4 > 0.$$

Therefore, under the stated condition, all eigenvalues of $J(P^*)$ have negative real parts, and P^* is locally asymptotically stable. □

Remark 10. *The nonlinear Beverton–Holt recruitment term couples the adult, nymphal, and larval populations through a density-dependent saturation mechanism. Owing to this nonlinear coupling, the construction of a global Lyapunov function for the coexistence equilibrium is not straightforward. Therefore, to establish the global dynamics of the system under the persistence condition $\mathcal{R}_0 > 1$, we use the uniform persistence theory together with the Li–Muldowney geometric approach, which provides a suitable framework for proving global asymptotic stability under weaker assumptions.*

3.8. Uniform persistence

We next investigate the long-term persistence of the mite population when the population reproduction threshold exceeds unity. Let

$$X = \mathbb{R}^4_+, \qquad X^\circ = \mathbb{R}^4_{++}, \qquad \partial X = X \setminus X^\circ,$$

and define

$$\phi(E, L, N, A) = \min\{E, L, N, A\}.$$

Theorem 11. *Assume that $\mathcal{R}_0 > 1$. Then System* (1) *is uniformly persistent in X°. More precisely, there is a constant $\xi > 0$, independent of the initial condition, such that every solution with initial data in X° satisfies*

$$\liminf_{t\to\infty} E(t) \geq \xi, \qquad \liminf_{t\to\infty} L(t) \geq \xi,$$
$$\liminf_{t\to\infty} N(t) \geq \xi, \qquad \liminf_{t\to\infty} A(t) \geq \xi.$$

Equivalently, we have

$$\liminf_{t\to\infty} \phi(x(t)) \geq \xi.$$

Proof. By Lemma 3 and Corollary 5, the semiflow generated by System (1) is point dissipative and possesses a compact absorbing set in X. Since the system is finite dimensional and its vector field is continuously differentiable, the semiflow is asymptotically smooth.

We first determine the maximal invariant subset of the boundary ∂X. Suppose that a complete trajectory remains entirely in ∂X. If $E = 0$, then

$$\dot{E} = \frac{\beta A}{1 + \dfrac{A + N + L}{K}}.$$

Therefore, invariance of the boundary face $E = 0$ requires $A = 0$. If $A = 0$, then

$$\dot{A} = \gamma_N N,$$

and hence invariance requires $N = 0$. Similarly, if $N = 0$, then

$$\dot{N} = \gamma_L L,$$

so invariance requires $L = 0$. Finally, if $L = 0$, then

$$\dot{L} = \gamma_E E,$$

which requires $E = 0$. Consequently, the origin

$$P_0 = (0, 0, 0, 0)$$

is the only invariant set contained in ∂X.

We next show that P_0 is a weak repeller for the interior semiflow. Since $\mathcal{R}_0 > 1$, one can choose $\varepsilon > 0$ to be sufficiently small such that

$$c_\varepsilon = \frac{1}{1 + \dfrac{\varepsilon}{K}} > \frac{1}{\mathcal{R}_0}.$$

Consider the neighborhood

$$U_\varepsilon = \{(E, L, N, A) \in X : A + N + L \leq \varepsilon\}.$$

For every $x \in U_\varepsilon$, we have

$$\frac{1}{1 + \dfrac{A + N + L}{K}} \geq c_\varepsilon.$$

Hence,

$$\dot{E} \geq \beta c_\varepsilon A - \alpha_1 E.$$

The remaining equations satisfy

$$\dot{L} = \gamma_E E - \alpha_2 L, \qquad \dot{N} = \gamma_L L - \alpha_3 N, \qquad \dot{A} = \gamma_N N - \mu_A A.$$

Thus, while a positive solution remains in U_ε, it dominates the cooperative linear system

$$\dot{y} = M_\varepsilon y, \tag{2}$$

where

$$M_\varepsilon = \begin{pmatrix} -\alpha_1 & 0 & 0 & \beta c_\varepsilon \\ \gamma_E & -\alpha_2 & 0 & 0 \\ 0 & \gamma_L & -\alpha_3 & 0 \\ 0 & 0 & \gamma_N & -\mu_A \end{pmatrix}.$$

The reproduction threshold associated with M_ε is

$$\mathcal{R}_\varepsilon = c_\varepsilon \mathcal{R}_0 > 1.$$

Therefore, the irreducible Metzler matrix M_ε has the following positive spectral bound:

$$s(M_\varepsilon) > 0.$$

It follows from the Perron–Frobenius theory for irreducible Metzler matrices that every positive solution of (2) grows in the direction of a strictly positive eigenvector. Hence, an interior trajectory of System (1) cannot remain indefinitely in U_ε. In particular, no solution starting in X° can converge to P_0.

Thus, P_0 is an isolated weak repeller for the interior semiflow. Since the semiflow is point dissipative and asymptotically smooth, and since P_0 is the only invariant set on the boundary, the standard uniform persistence theorem [24–27] implies that $\xi > 0$ exists such that

$$\liminf_{t \to \infty} \phi(x(t)) \geq \xi$$

for every solution with initial data in X°. □

Corollary 12. *If $\mathcal{R}_0 > 1$, then there is a compact absorbing set*

$$\Omega_* \subset X^\circ$$

for the semiflow restricted to X°. In particular, there are positive constants

$$\underline{E}, \quad \underline{L}, \quad \underline{N}, \quad \underline{A}, \quad M$$

such that every trajectory with initial data in X° eventually enters a compact positively invariant set Ω_* satisfying

$$\underline{E} \leq E \leq M, \qquad \underline{L} \leq L \leq M,$$
$$\underline{N} \leq N \leq M, \qquad \underline{A} \leq A \leq M.$$

3.9. Global stability via the Li–Muldowney criterion

We now derive a sufficient condition for the global asymptotic stability of the coexistence equilibrium using the geometric approach of Li and Muldowney [28].

Let

$$x = (E, L, N, A)^T$$

and write System (1) in the form

$$\dot{x} = h(x),$$

where

$$h_1(x) = \frac{\beta A}{1 + \dfrac{A + N + L}{K}} - \alpha_1 E, \quad h_2(x) = \gamma_E E - \alpha_2 L,$$
$$h_3(x) = \gamma_L L - \alpha_3 N, \quad h_4(x) = \gamma_N N - \mu_A A.$$

For convenience, define

$$q(x) = 1 + \frac{A + N + L}{K},$$

and

$$r(x) = \frac{\beta A}{K q(x)^2}, \qquad s(x) = \frac{\beta\left(1 + \dfrac{N + L}{K}\right)}{q(x)^2}.$$

Notice that $r(x) > 0, \quad s(x) > 0$.

The Jacobian matrix of h is

$$J(x) = \begin{pmatrix} -\alpha_1 & -r & -r & s \\ \gamma_E & -\alpha_2 & 0 & 0 \\ 0 & \gamma_L & -\alpha_3 & 0 \\ 0 & 0 & \gamma_N & -\mu_A \end{pmatrix}.$$

With respect to the ordered basis $(12, 13, 14, 23, 24, 34)$, the second additive compound matrix of J, constructed according to the standard definition in [29], is

$$J^{[2]}(x) = \begin{pmatrix} -(\alpha_1 + \alpha_2) & 0 & 0 & r & -s & 0 \\ \gamma_L & -(\alpha_1 + \alpha_3) & 0 & -r & 0 & -s \\ 0 & \gamma_N & -(\alpha_1 + \mu_A) & 0 & -r & -r \\ 0 & \gamma_E & 0 & -(\alpha_2 + \alpha_3) & 0 & 0 \\ 0 & 0 & \gamma_E & \gamma_N & -(\alpha_2 + \mu_A) & 0 \\ 0 & 0 & 0 & 0 & \gamma_L & -(\alpha_3 + \mu_A) \end{pmatrix}.$$

Choose the state-dependent diagonal matrix

$$P(x) = \operatorname{diag}\left(\frac{1}{L}, \frac{1}{N}, \frac{1}{A}, \frac{1}{LN}, \frac{1}{LA}, \frac{1}{NA}\right), \qquad x \in X^\circ.$$

The corresponding Bendixson matrix is

$$B(x) = P_f(x)P(x)^{-1} + P(x)J^{[2]}(x)P(x)^{-1},$$

where P_f denotes the directional derivative of P along the vector field.

Since

$$\frac{\dot{L}}{L} = \gamma_E \frac{E}{L} - \alpha_2, \qquad \frac{\dot{N}}{N} = \gamma_L \frac{L}{N} - \alpha_3,$$

and

$$\frac{\dot{A}}{A} = \gamma_N \frac{N}{A} - \mu_A,$$

a direct calculation gives

$$B(x) = \begin{pmatrix} -\alpha_1 - \gamma_E \frac{E}{L} & 0 & 0 & Nr & -As & 0 \\ \gamma_L \frac{L}{N} & -\alpha_1 - \gamma_L \frac{L}{N} & 0 & -Lr & 0 & -As \\ 0 & \gamma_N \frac{N}{A} & -\alpha_1 - \gamma_N \frac{N}{A} & 0 & -Lr & -Nr \\ 0 & \frac{\gamma_E}{L} & 0 & -\gamma_E \frac{E}{L} - \gamma_L \frac{L}{N} & 0 & 0 \\ 0 & 0 & \frac{\gamma_E}{L} & \gamma_N \frac{N}{A} & -\gamma_E \frac{E}{L} - \gamma_N \frac{N}{A} & 0 \\ 0 & 0 & 0 & 0 & \gamma_L \frac{L}{N} & -\gamma_L \frac{L}{N} - \gamma_N \frac{N}{A} \end{pmatrix}.$$

We use the Lozinskii measure associated with the vector 1-norm:

$$\mu_1(B) = \max_{1 \le j \le 6} \left(b_{jj} + \sum_{i \ne j} |b_{ij}| \right).$$

The corresponding column estimates are

$$\begin{aligned} C_1(x) &= -\alpha_1 - \gamma_E \frac{E}{L} + \gamma_L \frac{L}{N}, \\ C_2(x) &= -\alpha_1 - \gamma_L \frac{L}{N} + \gamma_N \frac{N}{A} + \frac{\gamma_E}{L}, \\ C_3(x) &= -\alpha_1 - \gamma_N \frac{N}{A} + \frac{\gamma_E}{L}, \\ C_4(x) &= -\gamma_E \frac{E}{L} - \gamma_L \frac{L}{N} + Nr + \gamma_N \frac{N}{A}, \\ C_5(x) &= -\gamma_E \frac{E}{L} - \gamma_N \frac{N}{A} + As + Lr + \gamma_L \frac{L}{N}, \\ C_6(x) &= -\gamma_L \frac{L}{N} - \gamma_N \frac{N}{A} + As + Nr. \end{aligned}$$

The functions r and s satisfy the global estimates

$$0 < r(x) \le \frac{\beta}{4}, \qquad 0 < s(x) \le \beta.$$

Indeed,

$$r(x) = \frac{\beta A}{K q(x)^2} \le \beta \frac{A/K}{(1 + A/K)^2} \le \frac{\beta}{4},$$

and

$$s(x) = \frac{\beta\left(1 + \dfrac{N+L}{K}\right)}{q(x)^2} \le \beta.$$

Let $\Omega_* \subset X^\circ$ be the compact absorbing set obtained in Corollary 12. On Ω_*, define the following upper bounds:

$$\begin{aligned}
\widehat{C}_1 &= -\alpha_1 - \gamma_E \frac{\underline{E}}{M} + \gamma_L \frac{M}{\underline{N}},\\
\widehat{C}_2 &= -\alpha_1 - \gamma_L \frac{\underline{L}}{M} + \gamma_N \frac{M}{\underline{A}} + \frac{\gamma_E}{\underline{L}},\\
\widehat{C}_3 &= -\alpha_1 - \gamma_N \frac{\underline{N}}{M} + \frac{\gamma_E}{\underline{L}},\\
\widehat{C}_4 &= -\gamma_E \frac{\underline{E}}{M} - \gamma_L \frac{\underline{L}}{M} + \frac{\beta M}{4} + \gamma_N \frac{M}{\underline{A}},\\
\widehat{C}_5 &= -\gamma_E \frac{\underline{E}}{M} - \gamma_N \frac{\underline{N}}{M} + \beta M + \frac{\beta M}{4} + \gamma_L \frac{M}{\underline{N}},\\
\widehat{C}_6 &= -\gamma_L \frac{\underline{L}}{M} - \gamma_N \frac{\underline{N}}{M} + \beta M + \frac{\beta M}{4}.
\end{aligned}$$

Theorem 13. *Assume the following:*

(1) $\mathcal{R}_0 > 1$*;*
(2) The coexistence equilibrium P^* *is locally asymptotically stable;*
(3) The estimates above satisfy

$$\widehat{C}_j < 0, \qquad j = 1, \dots, 6.$$

Then the coexistence equilibrium P^* *is globally asymptotically stable with respect to all initial data in* X°*.*

Proof. By Theorem 11 and Corollary 12, every trajectory starting in X° eventually enters the compact positively invariant set $\Omega_* \subset X^\circ$.

For every $x \in \Omega_*$, the column estimates satisfy

$$C_j(x) \le \widehat{C}_j, \qquad j = 1, \dots, 6.$$

Therefore, if

$$\widehat{C}_j < 0, \qquad j = 1, \dots, 6,$$

then a constant $\eta > 0$ exists such that

$$\mu_1(B(x)) = \max_{1 \le j \le 6} C_j(x) \le -\eta \qquad \text{for all } x \in \Omega_*.$$

Consequently, we have

$$\limsup_{t \to \infty} \frac{1}{t} \int_0^t \mu_1(B(x(s)))\, ds \le -\eta < 0.$$

The geometric Bendixson criterion of Li and Muldowney [28] therefore excludes nontrivial periodic orbits, homoclinic orbits, and invariant oriented phase polygons in Ω_*. Since $\mathcal{R}_0 > 1$, System (1) has a unique equilibrium P^* in X°. Moreover, P^* is locally asymptotically stable by assumption.

It follows from the Li–Muldowney global stability theorem that every trajectory starting in X° converges to P^*. Hence, we have

$$\lim_{t\to\infty}(E(t), L(t), N(t), A(t)) = P^*,$$

and P^* is globally asymptotically stable in X°. □

Remark 14. *The conditions*

$$\widehat{C}_j < 0, \qquad j = 1, \ldots, 6,$$

are sufficient conditions for the negativity of the Lozinskii measure. They are not necessary and may be conservative because they are obtained by replacing the state-dependent quantities with uniform upper and lower bounds on the absorbing set Ω_*. Numerical convergence to P^* for a parameter set that does not satisfy these inequalities should therefore be interpreted as numerical evidence for that parameter set, rather than as verification of Theorem 13.

3.10. Forward bifurcation at the extinction equilibrium

The local stability analysis shows that the extinction equilibrium P_0 is locally asymptotically stable when $\mathcal{R}_0 < 1$ and unstable when $\mathcal{R}_0 > 1$. At the critical value $\mathcal{R}_0 = 1$, the equilibrium becomes nonhyperbolic. To determine the direction of the bifurcation and characterize the transition from extinction to persistence, we apply the center manifold result of Castillo-Chavez and Song [30].

Theorem 15. *System* (1) *undergoes a forward transcritical bifurcation at the extinction equilibrium P_0 when $\mathcal{R}_0 = 1$.*

Proof. We choose β as the bifurcation parameter and use β^* to denote its critical value corresponding to $\mathcal{R}_0 = 1$. Since

$$\mathcal{R}_0 = \frac{\beta\gamma_E\gamma_L\gamma_N}{\alpha_1\alpha_2\alpha_3\mu_A},$$

the critical value is

$$\beta^* = \frac{\alpha_1\alpha_2\alpha_3\mu_A}{\gamma_E\gamma_L\gamma_N}.$$

At (P_0, β^*), the Jacobian matrix is

$$J(P_0, \beta^*) = \begin{pmatrix} -\alpha_1 & 0 & 0 & \beta^* \\ \gamma_E & -\alpha_2 & 0 & 0 \\ 0 & \gamma_L & -\alpha_3 & 0 \\ 0 & 0 & \gamma_N & -\mu_A \end{pmatrix}.$$

At $\mathcal{R}_0 = 1$, the constant term of the characteristic polynomial vanishes, and hence $\lambda = 0$ is an eigenvalue. Moreover, the remaining cubic factor satisfies the corresponding Routh–Hurwitz conditions established in the local stability analysis. Thus, the zero eigenvalue is simple, whereas the other three eigenvalues have negative real parts. Therefore, the center manifold theorem is applicable.

Let

$$w = (w_1, w_2, w_3, w_4)^T$$

be a right eigenvector associated with the zero eigenvalue. Choosing $w_1 = 1$, the relation

$$J(P_0, \beta^*)w = 0$$

gives

$$w = \left(1, \frac{\gamma_E}{\alpha_2}, \frac{\gamma_E\gamma_L}{\alpha_2\alpha_3}, \frac{\gamma_E\gamma_L\gamma_N}{\alpha_2\alpha_3\mu_A}\right)^T.$$

Similarly, let

$$v = (v_1, v_2, v_3, v_4)^T$$

be a left eigenvector corresponding to the zero eigenvalue. Before normalization, it may be chosen as

$$v = \left(1, \frac{\alpha_1}{\gamma_E}, \frac{\alpha_1\alpha_2}{\gamma_E\gamma_L}, \frac{\alpha_1\alpha_2\alpha_3}{\gamma_E\gamma_L\gamma_N}\right)^T.$$

We normalize v so that

$$v^T w = 1.$$

Since all components of v and w are positive, this normalization does not alter the signs of the bifurcation coefficients.

Write System (1) in the form

$$\dot{x} = h(x, \beta), \qquad x = (E, L, N, A)^T.$$

Following the center-manifold formulation of Castillo-Chavez and Song [30], define

$$a = \sum_{k,i,j=1}^{4} v_k w_i w_j \frac{\partial^2 h_k}{\partial x_i \partial x_j}(P_0, \beta^*)$$

and

$$b = \sum_{k,i=1}^{4} v_k w_i \frac{\partial^2 h_k}{\partial x_i \partial \beta}(P_0, \beta^*).$$

Only the first component, namely

$$h_1(x, \beta) = \frac{\beta A}{1 + \dfrac{A + N + L}{K}} - \alpha_1 E,$$

contains nonlinear terms. At P_0, its relevant second-order derivatives are

$$\frac{\partial^2 h_1}{\partial A^2} = -\frac{2\beta^*}{K}, \qquad \frac{\partial^2 h_1}{\partial A \partial L} = \frac{\partial^2 h_1}{\partial L \partial A} = -\frac{\beta^*}{K},$$

and

$$\frac{\partial^2 h_1}{\partial A \partial N} = \frac{\partial^2 h_1}{\partial N \partial A} = -\frac{\beta^*}{K}.$$

All other second-order derivatives with respect to the state variables vanish at P_0. Consequently, we have

$$\begin{aligned} a &= -\frac{2\beta^* v_1}{K}\left(w_4^2 + w_2 w_4 + w_3 w_4\right) \\ &= -\frac{2\beta^* v_1 w_4}{K}\left(w_2 + w_3 + w_4\right) < 0. \end{aligned}$$

Furthermore,

$$\left.\frac{\partial^2 h_1}{\partial A\, \partial \beta}\right|_{(P_0,\beta^*)} = 1,$$

whereas the remaining mixed derivatives involving β vanish at P_0. It follows that

$$b = v_1 w_4 > 0.$$

Therefore,

$$a < 0 \qquad \text{and} \qquad b > 0.$$

By the theorem of Castillo-Chavez and Song, a locally asymptotically stable positive equilibrium emerges for parameter values satisfying $\beta > \beta^*$; equivalently, $\mathcal{R}_0 > 1$. Since the extinction equilibrium branch exists for all values of β, the exchange of stability at $\mathcal{R}_0 = 1$ is a forward transcritical bifurcation. □

Remark 16. *The direction of the bifurcation is also consistent with the explicit expression*

$$A^* = \frac{K(\mathcal{R}_0 - 1)}{1 + C_L + C_N}.$$

Indeed, $A^* > 0$ precisely when $\mathcal{R}_0 > 1$, and A^* approaches zero as $\mathcal{R}_0$ approaches 1 from above. Since

$$E^* = C_E A^*, \qquad L^* = C_L A^*, \qquad N^* = C_N A^*,$$

all components of the coexistence equilibrium approach zero simultaneously. Hence, P^* approaches P_0 continuously as $\mathcal{R}_0$ approaches 1 from above, which provides an independent confirmation of the forward direction of the bifurcation.

4. Numerical simulation of the uncontrolled system

To complement the theoretical analysis presented in the previous section, we perform numerical simulations of the uncontrolled system using biologically plausible parameter values taken from Chaaban et al. [19] and summarized in Table 1. These values describe the developmental transition and mortality rates of the different life stages of *O. afrasiaticus* and provide a biologically meaningful basis for illustrating the qualitative dynamics of the proposed model. The simulations are designed to illustrate the threshold behavior governed by the population reproduction threshold $\mathcal{R}_0$. Since long-term field observations for all developmental stages are not currently available, the numerical results are intended to support the analytical findings rather than to provide a quantitative calibration or field validation of the model. All parameter values are kept fixed as listed in Table 1, except for the

oviposition rate β, which is varied to illustrate the extinction and coexistence regimes. For $\beta = 0.05$, we obtain $\mathcal{R}_0 = 0.4233 < 1$. Therefore, by Theorems 7 and 8, the extinction equilibrium P_0 is locally and globally asymptotically stable. This theoretical result is consistent with the numerical trajectories, which converge to P_0, as shown in the left-hand panel of Figure 2. For $\beta = 1.5$, the population reproduction threshold is $\mathcal{R}_0 = 12.6986 > 1$, and the corresponding coexistence equilibrium is

$$P^* = (448.6848,\ 169.9723,\ 175.6236,\ 824.2601).$$

Substituting these equilibrium values and the parameter values listed in Table 1 into the coefficients of the characteristic polynomial gives

$$\eta_1 = 1.108000, \qquad \eta_2 = 0.433066, \qquad \eta_3 = 0.072543, \qquad \eta_4 = 0.002492.$$

Furthermore,

$$\Delta_3 = \eta_1\eta_2\eta_3 - \eta_3^2 - \eta_1^2\eta_4 = 0.026488 > 0.$$

Thus, all four coefficients are positive, and the Liénard–Chipart condition stated in Theorem 9 is satisfied. Consequently, the coexistence equilibrium P^* is locally asymptotically stable for the parameter set used in this simulation. The numerical trajectories converge to the same analytically calculated equilibrium, as illustrated in the right-hand panel of Figure 2. Overall, Figure 2 illustrates the threshold dynamics predicted by the analytical results: Extinction occurs when $\mathcal{R}_0 < 1$, whereas a positive persistent population is observed when $\mathcal{R}_0 > 1$.

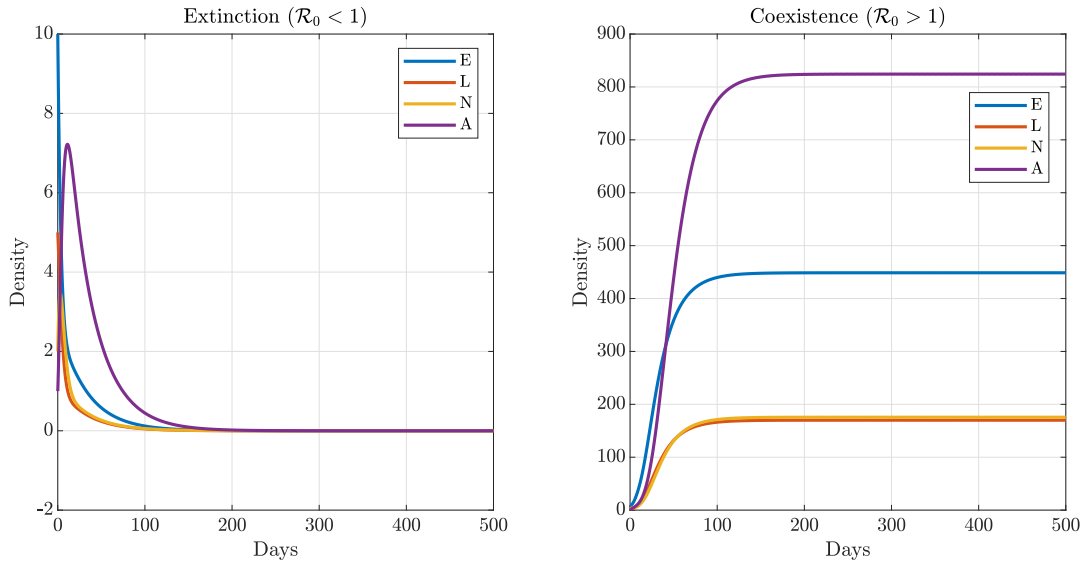

Figure 2. Numerical trajectories of the uncontrolled system in the extinction and coexistence regimes. For $\beta = 0.05$, $\mathcal{R}_0 < 1$ and the trajectories converge to P_0; for $\beta = 1.5$, $\mathcal{R}_0 > 1$ and the trajectories converge to P^*.

It should be emphasized that the numerical parameter set used in the coexistence simulation satisfies the hypotheses of the local stability result but is not claimed to satisfy the sufficient conditions of Theorem 13. Those global stability conditions are conservative and constitute an independent sufficient criterion. Accordingly, the observed convergence to P^* should be interpreted as numerical evidence

for the selected parameter set rather than as a numerical verification of the global asymptotic stability theorem.

The bifurcation diagram displayed in Figure 3 illustrates the forward transcritical bifurcation established analytically in Theorem 15. The extinction equilibrium is stable for $\mathcal{R}_0 < 1$ and loses stability at the critical value $\mathcal{R}_0 = 1$, where the positive coexistence branch emerges into the region $\mathcal{R}_0 > 1$.

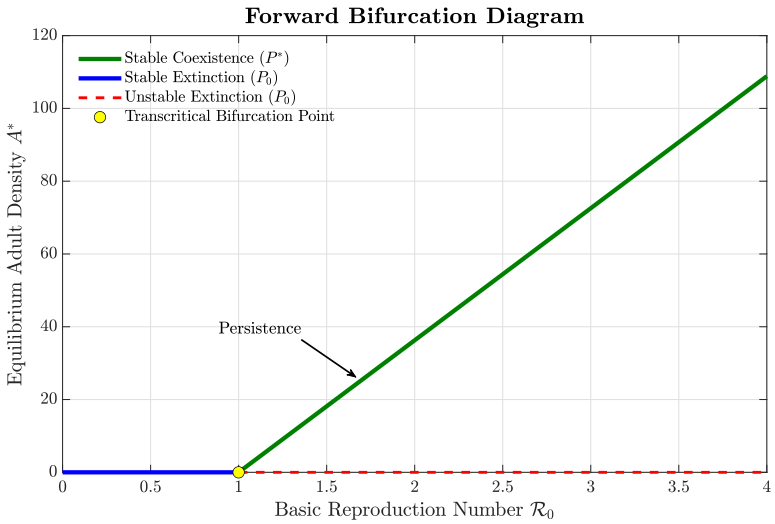

Figure 3. Forward transcritical bifurcation at $\mathcal{R}_0 = 1$. The extinction and coexistence regimes correspond to $\mathcal{R}_0 < 1$ and $\mathcal{R}_0 > 1$, respectively.

Biologically, the forward direction of the bifurcation implies that the critical value $\mathcal{R}_0 = 1$ separates the extinction and persistence regimes within the proposed model. Since no positive coexistence equilibrium exists for $\mathcal{R}_0 < 1$, reducing the population reproduction threshold below unity guarantees convergence to the extinction equilibrium within the mathematical framework of the model, without the additional complications associated with backward bifurcation.

Sensitivity analysis

To further assess the influence of the model parameters on the system dynamics, we perform a local sensitivity analysis of the uncontrolled System (1). The normalized forward sensitivity index is used to quantify the relative effect of each parameter on a selected model output. It is defined by

$$\Upsilon_{\Psi}^{\theta} = \frac{\partial \Psi}{\partial \theta} \frac{\theta}{\Psi},$$

where Ψ denotes the output quantity of interest and θ is a model parameter.

Since analytical expressions for the required derivatives are not always available, the sensitivity indices are approximated numerically using a forward finite difference scheme:

$$\Upsilon_{\Psi}^{\theta} \approx \frac{\Psi(\theta + \delta\theta) - \Psi(\theta)}{\delta\, \Psi(\theta)}, \qquad 0 < \delta \ll 1.$$

Two model outputs are considered in the analysis: The population reproduction threshold $\mathcal{R}_0$ and the total equilibrium infestation burden

$$Q^* = E^* + L^* + N^* + A^*.$$

A positive sensitivity index indicates that increasing a parameter increases the corresponding model output, whereas a negative index indicates that the output decreases as the parameter increases. The larger the absolute value of the sensitivity index, the greater the influence of the corresponding parameter. The computed sensitivity indices are summarized in Table 3.

Table 3. Normalized sensitivity indices of the date palm mite model parameters.

Parameter	Nominal value	$\Upsilon_\theta^{\mathcal{R}_0}$	$\Upsilon_\theta^{Q^*}$
β	1.5	1	1.08548
γ_E	0.161	0.25806	0.00291
γ_L	0.404	0.04941	0.08022
γ_N	0.352	0.09974	0.12625
μ_E	0.056	-0.25806	-0.28012
μ_L	0.021	-0.04941	-0.03994
μ_N	0.039	-0.09974	-0.08464
μ_A	0.0750	-1	-0.89016
K	100	0	1

The sensitivity indices presented in Table 3 indicate that the oviposition rate β is the most influential parameter affecting both the population reproduction threshold $\mathcal{R}_0$ and the total equilibrium infestation burden Q^*. Specifically, a 1% increase in β results in an approximately 1% increase in $\mathcal{R}_0$ and a 1.085% increase in Q^*. Conversely, the adult mortality rate μ_A has the strongest negative influence on both quantities, with normalized sensitivity indices of -1 for $\mathcal{R}_0$ and approximately -0.890 for Q^*. This finding highlights the crucial role of adult survival in determining the long-term persistence of the mite population and suggests that management strategies targeting the adult stage are likely to be the most effective. The saturation parameter K has no influence on $\mathcal{R}_0$, since the density-dependent saturation term does not appear in the linearization of the system at the extinction equilibrium. However, it exerts a strong positive influence on Q^*, with a normalized sensitivity index equal to one. Consequently, increasing K weakens the density-dependent limitation on egg production and allows a larger equilibrium infestation level. The developmental transition rates γ_E, γ_L, and γ_N all have positive sensitivity indices with respect to $\mathcal{R}_0$, indicating that faster progression through the immature stages promotes the population's persistence. Their influence on Q^*, however, differs substantially. Among these parameters, γ_N has the largest positive effect, followed by γ_L, whereas the effect of γ_E on Q^* is almost negligible for the nominal parameter set. The mortality rates μ_E, μ_L, and μ_N all reduce both $\mathcal{R}_0$ and Q^*, with egg mortality μ_E producing the largest reduction among the immature-stage mortality parameters. Overall, the sensitivity analysis demonstrates that the long-term dynamics of the model are primarily governed by the oviposition rate β, the adult mortality rate μ_A, and the saturation parameter K. These findings are illustrated in Figures 4 and 5.

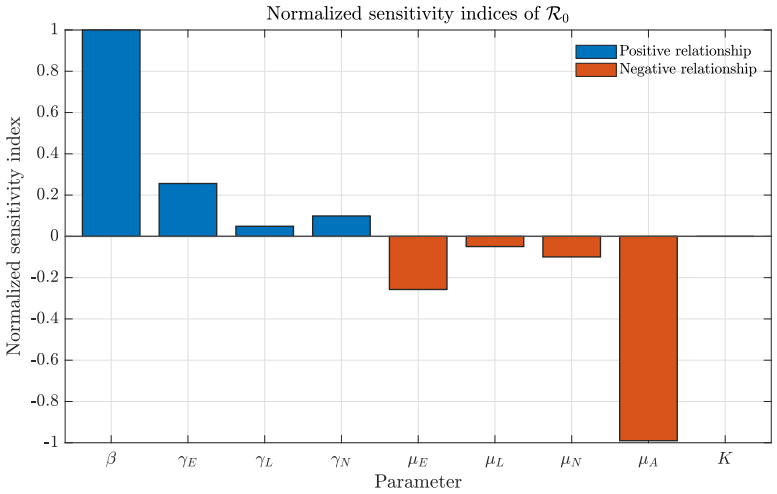

Figure 4. Sensitivity analysis of $\mathcal{R}_0$.

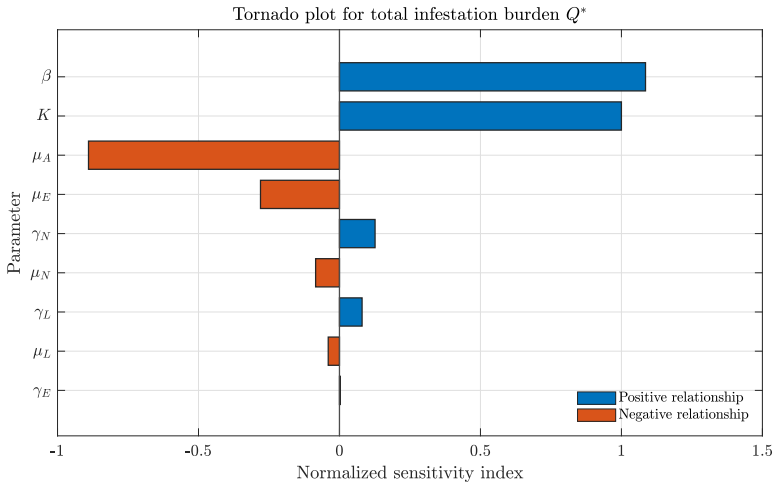

Figure 5. Sensitivity analysis of the equilibrium infestation burden Q^*.

5. Optimal control analysis

To investigate effective strategies for mitigating date palm mite infestations while accounting for the associated implementation costs, we incorporate three time-dependent control functions into System (1). The resulting controlled model is given by

$$\begin{cases} \dfrac{dE}{dt} = \dfrac{\beta A}{1 + \dfrac{A+N+L}{K}} - (\gamma_E + \mu_E + u_1 + u_3)E, \\ \dfrac{dL}{dt} = \gamma_E E - (\gamma_L + \mu_L + u_1 + u_3)L, \\ \dfrac{dN}{dt} = \gamma_L L - (\gamma_N + \mu_N + u_2 + u_3)N, \\ \dfrac{dA}{dt} = \gamma_N N - (\mu_A + u_2 + u_3)A. \end{cases} \tag{3}$$

The control variables $u_1(t)$, $u_2(t)$, and $u_3(t)$ represent the time-dependent intensities of the mechanical, biological, and chemical control measures, respectively. Mechanical control is assumed to reduce the egg and larval populations through sanitation and the removal of infested plant material. Biological control targets the nymph and adult stages through the action of natural enemies, whereas chemical control acts on all developmental stages by increasing their mortality rates.

The set of admissible controls is defined by

$$\mathcal{U} = \left\{(u_1, u_2, u_3) : [0, T] \to \mathbb{R}^3 \text{ measurable} : \ 0 \le u_i(t) \le 1, \ i = 1, 2, 3, \ t \in [0, T]\right\}.$$

The objective is to minimize the total mite population while simultaneously reducing the implementation costs associated with the three control measures. Accordingly, the objective functional is defined as

$$J(u_1, u_2, u_3) = \int_0^T \left[A_1 E(t) + A_2 L(t) + A_3 N(t) + A_4 A(t) + \frac{B_1}{2}u_1^2(t) + \frac{B_2}{2}u_2^2(t) + \frac{B_3}{2}u_3^2(t)\right] dt. \tag{4}$$

Here, $A_1, A_2, A_3, A_4 > 0$ are the weighting coefficients associated with the egg, larval, nymphal, and adult stages of the mite population, respectively, whereas $B_1, B_2, B_3 > 0$ represent the relative costs of implementing the mechanical, biological, and chemical control measures. The coefficients A_i allow different developmental stages to be assigned different levels of importance according to their biological or economic impact, while the coefficients B_i balance the benefits of control against the corresponding implementation costs.

Theorem 17. *There is an optimal control triple*

$$(u_1^*, u_2^*, u_3^*) \in \mathcal{U}$$

such that

$$J(u_1^*, u_2^*, u_3^*) = \min_{(u_1,u_2,u_3)\in\mathcal{U}} J(u_1, u_2, u_3).$$

Proof. The existence of an optimal control follows from the standard existence theorem of Fleming and Rishel [31]. The set of admissible controls $\mathcal{U}$ is nonempty, closed, bounded, and convex in $L^\infty([0, T])^3$. Furthermore, the right-hand side of the controlled system is continuously differentiable with respect to the state variables and affine with respect to the control variables. Consequently, it is locally Lipschitz continuous with respect to the state variables, which guarantees the existence of a unique state solution

for every admissible control. Moreover, the integrand of the objective functional is continuous, convex with respect to the control variables, and bounded below by the quadratic function

$$\frac{B_1}{2}u_1^2 + \frac{B_2}{2}u_2^2 + \frac{B_3}{2}u_3^2.$$

Since the state variables remain bounded on the finite interval $[0, T]$, all the hypotheses of the Fleming–Rishel existence theorem are satisfied. Therefore, there is an optimal control

$$(u_1^*, u_2^*, u_3^*) \in \mathcal{U}$$

that minimizes the objective functional J. □

If we apply Pontryagin's maximum principle for bounded measurable controls [31–33], the Hamiltonian is defined by

$$\begin{aligned}\mathcal{H} = {} & A_1E + A_2L + A_3N + A_4A + \frac{B_1}{2}u_1^2 + \frac{B_2}{2}u_2^2 + \frac{B_3}{2}u_3^2 \\ & + \lambda_1\left[\frac{\beta A}{q} - (\gamma_E + \mu_E + u_1 + u_3)E\right] \\ & + \lambda_2\left[\gamma_E E - (\gamma_L + \mu_L + u_1 + u_3)L\right] \\ & + \lambda_3\left[\gamma_L L - (\gamma_N + \mu_N + u_2 + u_3)N\right] \\ & + \lambda_4\left[\gamma_N N - (\mu_A + u_2 + u_3)A\right].\end{aligned} \tag{5}$$

The adjoint variables $\lambda_1, \lambda_2, \lambda_3, \lambda_4$ satisfy

$$\begin{cases}\dot{\lambda}_1 = -A_1 + (\gamma_E + \mu_E + u_1 + u_3)\lambda_1 - \gamma_E\lambda_2, \\ \dot{\lambda}_2 = -A_2 + \dfrac{\beta A}{Kq^2}\lambda_1 + (\gamma_L + \mu_L + u_1 + u_3)\lambda_2 - \gamma_L\lambda_3, \\ \dot{\lambda}_3 = -A_3 + \dfrac{\beta A}{Kq^2}\lambda_1 + (\gamma_N + \mu_N + u_2 + u_3)\lambda_3 - \gamma_N\lambda_4, \\ \dot{\lambda}_4 = -A_4 - \dfrac{\beta\left(1 + \dfrac{N+L}{K}\right)}{q^2}\lambda_1 + (\mu_A + u_2 + u_3)\lambda_4.\end{cases} \tag{6}$$

The transversality conditions are

$$\lambda_1(T) = 0, \qquad \lambda_2(T) = 0, \qquad \lambda_3(T) = 0, \qquad \lambda_4(T) = 0.$$

The optimal controls are obtained from the stationarity conditions

$$\frac{\partial \mathcal{H}}{\partial u_i} = 0, \qquad i = 1, 2, 3,$$

together with the bounds $0 \le u_i(t) \le 1$. Therefore, the optimal controls are characterized by

$$u_1^*(t) = \min\left\{1, \max\left[0, \frac{\lambda_1(t)E(t) + \lambda_2(t)L(t)}{B_1}\right]\right\}, \tag{7}$$

$$u_2^*(t) = \min\left\{1,\ \max\left[0,\ \frac{\lambda_3(t)N(t) + \lambda_4(t)A(t)}{B_2}\right]\right\}, \tag{8}$$

$$u_3^*(t) = \min\left\{1,\ \max\left[0,\ \frac{\lambda_1(t)E(t) + \lambda_2(t)L(t) + \lambda_3(t)N(t) + \lambda_4(t)A(t)}{B_3}\right]\right\}. \tag{9}$$

5.1. Numerical implementation of the optimality system

The optimality system, consisting of the controlled state equations, the adjoint equations, the transversality conditions, and the characterizations of the optimal controls, was solved numerically using the forward–backward sweep method. The state equations were integrated forward in time from the prescribed initial conditions, whereas the adjoint equations were integrated backward in time from the terminal conditions

$$\lambda_i(T) = 0, \qquad i = 1, 2, 3, 4.$$

Both integrations were performed using the classical fourth-order Runge–Kutta method.

The simulations were carried out over the finite control horizon

$$0 \le t \le T, \qquad T = 60 \text{ days},$$

using $N = 1200$ uniform time subintervals, yielding the fixed time step

$$\Delta t = \frac{T}{N} = 0.05 \text{ days}.$$

The initial population densities were chosen as

$$E(0) = 10, \qquad L(0) = 8, \qquad N(0) = 6, \qquad A(0) = 5.$$

The state-related weighting coefficients in the objective functional were selected as

$$A_1 = 1, \qquad A_2 = 1, \qquad A_3 = 2, \qquad A_4 = 3,$$

where the larger weights assigned to the nymphal and adult stages reflect their greater contribution to infestation development and spread. The corresponding control-cost coefficients were taken as

$$B_1 = 10, \qquad B_2 = 40, \qquad B_3 = 80,$$

which represent the relative implementation costs of the mechanical, biological, and chemical interventions, respectively.

The admissible controls satisfy

$$0 \le u_i(t) \le 1, \qquad i = 1, 2, 3.$$

For each active control, the forward–backward iteration was initialized with the constant profile

$$u_i^{(0)}(t) = 0.2,$$

whereas the inactive controls were kept identically equal to zero.

After each forward–backward iteration, the controls were projected onto their admissible intervals and updated according to the relaxation formula

$$u_i^{(k+1)} = \omega \widetilde{u}_i^{(k+1)} + (1-\omega) u_i^{(k)}, \qquad \omega = 0.5,$$

where $\widetilde{u}_i^{(k+1)}$ denotes the projected control obtained from the optimality conditions. The iterative process was terminated when

$$\max_{i=1,2,3} \left\| u_i^{(k+1)} - u_i^{(k)} \right\|_\infty < 10^{-7},$$

or after a maximum of 300 iterations.

The numerical values and computational settings used throughout the optimal control simulations are summarized in Table 4. All computations were performed in MATLAB R2020a.

Table 4. Numerical settings used in the optimal control simulations.

Quantity	**Value**
Control horizon T	60 days
Number of time subintervals N	1200
Time step Δt	0.05 days
Initial state (E_0, L_0, N_0, A_0)	$(10, 8, 6, 5)$
State weights (A_1, A_2, A_3, A_4)	$(1, 1, 2, 3)$
Control cost weights (B_1, B_2, B_3)	$(10, 40, 80)$
Control bounds	$0 \le u_i(t) \le 1$
Initial active control level	0.2
Relaxation parameter ω	0.5
Convergence tolerance	10^{-7}
Maximum number of iterations	300

5.2. Optimal control simulations

Using the numerical implementation described above, we now investigate the effectiveness of the proposed optimal control strategy. The objective is to minimize the weighted infestation burden while simultaneously reducing the implementation cost associated with the control measures.

Figure 6 compares the uncontrolled and optimally controlled population dynamics. In the absence of control, the system converges to the positive coexistence equilibrium, indicating the long-term persistence of the mite population. In contrast, the optimal control strategy substantially suppresses all developmental stages, driving the population toward extinction within a relatively short period. These results demonstrate that the proposed intervention strategy is capable of effectively eliminating the infestation when implemented according to the optimality conditions.

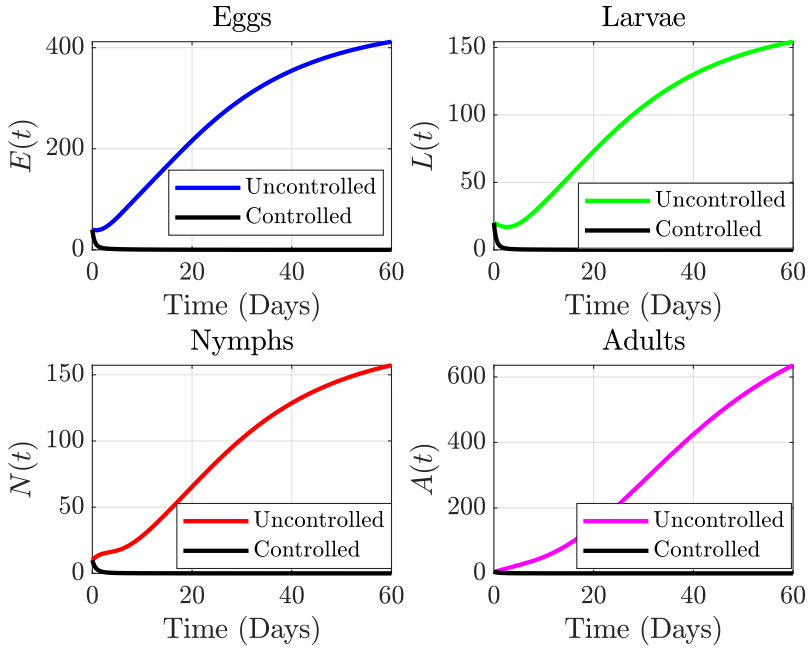

Figure 6. Population dynamics with and without optimal control.

Practical implementation. The optimal control profiles provide time-dependent recommendations for implementing integrated pest management rather than prescribing fixed intervention levels. Specifically, $u_1(t)$ represents mechanical measures, such as sanitation practices and the removal of infested fruits during the early stages of infestation. The control $u_2(t)$ corresponds to biological control through the release or conservation of natural enemies targeting the nymphal and adult stages, whereas $u_3(t)$ represents the application of chemical acaricides. The numerical results indicate that control efforts should be applied more intensively during the initial phase of infestation and then gradually reduced as the pest population declines. Such a strategy achieves effective suppression while avoiding unnecessary intervention costs, thereby providing a practical guideline for integrated pest management programs. It should be emphasized that these results describe the suppression of the mite population over the finite control horizon considered in the optimal control problem. They should not be interpreted as proving permanent eradication of the pest population under practical field conditions.

5.3. Cost-effectiveness analysis

A cost-effectiveness analysis was conducted to compare the economic performance of the seven intervention strategies considered in this study: u_1 only, u_2 only, u_3 only, $u_1 + u_2$, $u_1 + u_3$, $u_2 + u_3$, and $u_1 + u_2 + u_3$. For each strategy, the reduction in the weighted infestation burden was evaluated relative to the uncontrolled system, and the corresponding intervention cost was calculated over the finite control horizon $[0, T]$. Let

$$\mathcal{B}_0 = \int_0^T [A_1 E_0(t) + A_2 L_0(t) + A_3 N_0(t) + A_4 A_0(t)]\, dt$$

denote the cumulative weighted infestation burden associated with the uncontrolled trajectory. For the jth intervention strategy, the corresponding cumulative weighted burden is defined by

$$\mathcal{B}_j = \int_0^T \left[A_1 E_j(t) + A_2 L_j(t) + A_3 N_j(t) + A_4 A_j(t)\right] dt.$$

The total averted weighted infestation burden under strategy j is therefore given by

$$T_a^{(j)} = \mathcal{B}_0 - \mathcal{B}_j.$$

The total implementation cost associated with strategy j is calculated as

$$T_c^{(j)} = \int_0^T \left[\frac{B_1}{2} u_{1,j}^2(t) + \frac{B_2}{2} u_{2,j}^2(t) + \frac{B_3}{2} u_{3,j}^2(t)\right] dt.$$

All time integrals involved in the calculation of the infestation burden and intervention cost were evaluated numerically using the composite trapezoidal rule.

The average cost-effectiveness ratio (ACER) associated with strategy j is defined as

$$\mathrm{ACER}_j = \frac{T_c^{(j)}}{T_a^{(j)}}.$$

A smaller ACER indicates that a larger reduction in the weighted infestation burden is achieved per unit intervention cost.

To compare strategies with increasing effectiveness, the incremental cost-effectiveness ratio (ICER) was calculated as

$$\mathrm{ICER}_{j,i} = \frac{T_c^{(j)} - T_c^{(i)}}{T_a^{(j)} - T_a^{(i)}},$$

where strategy j is more effective than strategy i. The ICER therefore measures the additional cost required to obtain one additional unit of averted weighted infestation burden when moving from strategy i to strategy j.

A strategy was classified as strongly dominated if another strategy produced an equal or greater reduction in infestation at an equal or lower cost, with at least one of these inequalities being strict. Strongly dominated strategies were excluded before constructing the efficient frontier and calculating the sequential ICER values.

The cost-effectiveness results for all seven intervention strategies are presented in Table 5.

Table 5 shows that the three single-control strategies u_1, u_2, and u_3 are strongly dominated. Although these strategies reduce the infestation burden, each is outperformed by at least one combined strategy that achieves a greater reduction at a lower implementation cost. The strategy $u_1 + u_2 + u_3$ is also strongly dominated because its intervention cost is considerably higher than those of the non-dominated combined strategies without a corresponding improvement in effectiveness. After excluding the strongly dominated alternatives, the remaining strategies form the efficient frontier reported in Table 6. The strategies are ordered according to increasing effectiveness, and the ICER values are calculated sequentially along this frontier. The ICER values were computed using the full-precision numerical outputs before rounding the values reported in the table.

Table 5. Cost-effectiveness analysis of the proposed control strategies.

Strategy	T_a	T_c	ACER	Dominance status
u_1 only	72981	283.64	0.0038865	Strongly dominated
u_2 only	73944	615.06	0.0083179	Strongly dominated
u_3 only	74455	203.77	0.0027368	Strongly dominated
$u_1 + u_2$	74469	159.05	0.0021357	Non-dominated
$u_1 + u_3$	74456	141.45	0.0018997	Non-dominated
$u_2 + u_3$	74468	143.68	0.0019295	Non-dominated
$u_1 + u_2 + u_3$	74469	375.66	0.0050446	Strongly dominated

Table 6. Efficient frontier of the non-dominated control strategies.

Strategy	T_a	T_c	ACER	ICER
$u_1 + u_3$	74456	141.45	0.0018997	Reference
$u_2 + u_3$	74468	143.68	0.0019295	0.19886
$u_1 + u_2$	74469	159.05	0.0021357	8.8192

Note: The ICER values were calculated using the full-precision numerical outputs generated by the MATLAB code, whereas the values of T_a and T_c displayed in the table were rounded for presentation.

Among the non-dominated strategies, the combined mechanical and chemical intervention $u_1 + u_3$ has the lowest ACER, namely

$$\text{ACER} = 0.0018997,$$

and therefore provides the largest reduction in the weighted infestation burden per unit cost among the strategies considered.

The combined biological and chemical strategy $u_2 + u_3$ produces a slightly greater reduction in infestation than $u_1 + u_3$. Moving from $u_1 + u_3$ to $u_2 + u_3$ requires an incremental cost of 0.19886 per additional unit of averted weighted infestation burden. Thus, $u_2 + u_3$ may be considered when a decision-maker is willing to incur a modest additional cost to obtain a small improvement in effectiveness.

The strategy u_1+u_2 achieves the greatest averted burden among the strategies on the efficient frontier. However, its additional benefit relative to $u_2 + u_3$ is very small, whereas its ICER is substantially larger

$$\text{ICER} = 8.8192.$$

Consequently, the additional effectiveness provided by $u_1 + u_2$ comes at a comparatively high incremental cost. In the absence of a prescribed willingness-to-pay threshold, $u_1 + u_3$ may be regarded as the preferred strategy according to the minimum ACER criterion. It provides the most favorable balance between infestation reduction and intervention cost. Nevertheless, the final choice between the strategies on the efficient frontier may depend on the decision-maker's willingness to pay for an additional unit of averted weighted infestation burden.

6. Conclusions and discussion

In this paper, we developed and analyzed a stage-structured mathematical model describing the population dynamics of the date palm mite *O. afrasiaticus*. The model incorporates a Beverton–Holt density-dependent recruitment function to represent the reduction in egg production caused by resource limitation while preserving biological feasibility. The model explicitly accounts for the transitions among the egg, larval, nymphal, and adult stages. Analytical and numerical investigations were carried out to characterize the qualitative dynamics of the system and to evaluate effective management strategies. The theoretical analysis showed that the population reproduction threshold $\mathcal{R}_0$ governs the qualitative behavior of the system. When $\mathcal{R}_0 < 1$, the extinction equilibrium is locally and globally asymptotically stable, whereas a unique coexistence equilibrium exists for $\mathcal{R}_0 > 1$. Furthermore, the model undergoes a forward bifurcation at the critical threshold $\mathcal{R}_0 = 1$, indicating a continuous transition from extinction to persistent infestation. The numerical simulations are fully consistent with these analytical results and clearly illustrate the predicted threshold dynamics. The sensitivity analysis identified the oviposition rate β and the adult mortality rate μ_A as the parameters with the greatest influence on both the population reproduction threshold $\mathcal{R}_0$ and the equilibrium infestation burden Q^*. In contrast, the saturation parameter K does not influence $\mathcal{R}_0$, although it has a pronounced positive effect on the long-term equilibrium infestation level. These findings suggest that management practices aimed at reducing adult reproduction and increasing adult mortality are likely to be the most effective for limiting the long-term persistence of the mite population. The optimal control analysis demonstrated that the proposed integrated control measures substantially reduce the mite population over the prescribed finite control horizon. Compared with the uncontrolled system, the controlled trajectories exhibit a rapid decline in all developmental stages, indicating that appropriately timed interventions can effectively suppress infestation while reducing the overall implementation cost. It should be emphasized that these results describe the population's suppression over the finite simulation period considered in the optimal control problem and should not be interpreted as demonstrating permanent eradication of the pest population under field conditions. From an economic perspective, the cost-effectiveness analysis identified the combined mechanical and chemical strategy ($u_1 + u_3$) as the most cost-effective intervention according to the ACER. Although the combined biological and chemical strategy ($u_2 + u_3$) achieved a slightly greater reduction in infestation, the additional benefit was obtained at a higher incremental cost. The dominance analysis further showed that the remaining strategies were economically inferior because they were either more expensive or less effective than one or more competing strategies. Consequently, within the assumptions of the present model, the combined mechanical and chemical intervention provides the most favorable balance between biological effectiveness and implementation cost. Taken together, the analytical results, sensitivity analysis, optimal control simulations, and cost-effectiveness evaluation provide a comprehensive mathematical framework for studying the population dynamics of *O. afrasiaticus*. The proposed model may serve as a useful theoretical tool for evaluating alternative integrated pest management strategies and for supporting future quantitative decision- making when complemented with field observations and parameter calibration. Future work may extend the present model by incorporating discrete or distributed time delays to account for developmental and maturation periods. Such extensions are known to generate richer dynamical behaviors, including periodic oscillations and stability switches [34]. In addition, although the present numerical simulations are based on

experimentally reported biological parameters, future research will focus on calibrating the model using long-term field data to improve its predictive capability under different environmental conditions.

Author contributions

Saleh Aljurbua: Methodology, software, investigation, writing–original draft, writing–review and editing; Moustafa El-Shahed: Conceptualization, methodology, investigation, writing–original draft, writing–review and editing. All authors have read and agreed to the published version of the manuscript.

Use of Generative-AI tools declaration

The authors declare they have not used Artificial Intelligence (AI) tools in the creation of this article.

Acknowledgments

The Researchers would like to thank the Deanship of Graduate Studies and Scientific Research at Qassim University (www.qu.edu.sa) for financial support (QU-APC-2026).

Conflict of interest

The authors declare no conflicts of interest.

References

1. S. Ben Chaaban, S. Ben Maachia, Z. Rached, K. Mahjoubi, A. Namsi, Integrated pest management strategies for *Oligonychus afrasiaticus* (Acari: Tetranychidae) in Tunisia, *Euro-Mediterr. J. Environ. Integr.*, **10** (2025), 5115–5128. https://doi.org/10.1007/s41207-025-00898-9
2. M. Mohammed, H. El-Shafie, M. Munir, Development and validation of innovative machine learning models for predicting date palm mite infestation on fruits, *Agronomy*, **13** (2023), 494. https://doi.org/10.3390/agronomy13020494
3. J. H. Mirza, M. Kamran, F. J. Alatawi, Phenology and abundance of date palm mite *Oligonychus afrasiaticus* (McGregor) (Acari: Tetranychidae) in Riyadh, Saudi Arabia, *Saudi J. Biol. Sci.*, **28** (2021), 4348–4357. https://doi.org/10.1016/j.sjbs.2021.04.023
4. L. R. Jeppson, H. H. Keifer, E. W. Baker, *Mites injurious to economic plants*, Berkeley: University of California Press, 1975. https://doi.org/10.1525/9780520335431
5. E. M. Yahia, A. A. Kader, Date (*Phoenix dactylifera* L.), In: *Postharvest biology and technology of tropical and subtropical fruits*, Elsevier, 2011. https://doi.org/10.1533/9780857092885.41
6. S. A. Ghani, M. M. Al-Azzazy, S. S. Alhewairini, M. A. Al-Deghairi, The miticidal activity of silver nanoparticles towards date palm mite (*Oligonychus afrasiaticus* (McGregor)): efficacy, selectivity, and risk assessment, *Braz. J. Biol.*, **84** (2024), e261262. https://doi.org/10.1590/1519-6984.261262

7. S. A. Aldosari, Occurrence of dust mite, *Oligonychus afrasiaticus* on fruits, leaflets of some date palm trees and evaluation the efficiency of botanical compound (BIACO) as compared with some acaricides, *Assiut Univ. Bull. Environ. Res.*, **12** (2009), 69–76.

8. F. J. Alatawi, Field studies on occurrence, alternate hosts and mortality factors of date palm mite, *Oligonychus afrasiaticus* (McGregor) (Acari: Tetranychidae), *J. Saudi Soc. Agric. Sci.*, **19** (2020), 146–150. https://doi.org/10.1016/j.jssas.2018.08.003

9. L. Zhu, T. Zheng, Pattern dynamics analysis and application of West Nile virus spatiotemporal models based on higher-order network topology, *Bull. Math. Biol.*, **87** (2025), 121. https://doi.org/10.1007/s11538-025-01501-6

10. J. Shi, L. Zhu, Turing pattern theory on homogeneous and heterogeneous higher-order temporal network system, *J. Math. Phys.*, **66** (2025), 042706. https://doi.org/10.1063/5.0211728

11. C. I. Nkeki, I. A. Mbarie, On mathematical study of juvenile delinquency with precautionary measure, public education and intervention programs as control strategies, *J. Nonlinear Dyn. Appl.*, **2** (2026), 20–38. https://doi.org/10.62762/JNDA.2025.195550

12. Y. K. Park, Y. Nam, W. I. Choi, Modeling pine caterpillar, *Dendrolimus spectabilis* (Lepidoptera: Lasiocampidae), population dynamics with a stage-structured matrix model based on field observations, *Insects*, **17** (2026), 56. https://doi.org/10.3390/insects17010056

13. M. Pobożniak, M. Olczyk, Biocontrol in integrated pest management in fruit and vegetable field production, *Horticulturae*, **11** (2025), 522. https://doi.org/10.3390/horticulturae11050522

14. I. R. Fitri, F. Hanum, A. Kusnanto, T. Bakhtiar, Optimal pest control strategies with cost-effectiveness analysis, *Sci. World J.*, **2021** (2021), 6630193. https://doi.org/10.1155/2021/6630193

15. W. Zhou, Y. Arcot, R. F. Medina, J. Bernal, L. Cisneros-Zevallos, M. E. S. Akbulut, Integrated pest management: an update on the sustainability approach to crop protection, *ACS Omega*, **9** (2024), 41130–41147. https://doi.org/10.1021/acsomega.4c06628

16. R. J. H. Beverton, S. J. Holt, *On the dynamics of exploited fish populations*, Ministry of Agriculture, Fisheries and Food, Fisheries Investigations, Series II, Vol. 19, 1957.

17. H. K. Kindsvater, M. Mangel, J. D. Reynolds, N. K. Dulvy, Ten principles from evolutionary ecology essential for effective marine conservation, *Ecol. Evol.*, **6** (2016), 2125–2138. https://doi.org/10.1002/ece3.2012

18. B. van Poorten, J. Korman, C. Walters, Revisiting Beverton–Holt recruitment in the presence of variation in food availability, *Rev. Fish Biol. Fish.*, **28** (2018), 607–624. https://doi.org/10.1007/s11160-018-9521-6

19. S. Ben Chaaban, B. Chermiti, S. Kreiter, Comparative demography of the spider mite, *Oligonychus afrasiaticus*, on four date palm varieties in southwestern Tunisia, *J. Insect Sci.*, **11** (2011), 136. https://doi.org/10.1673/031.011.13601

20. E. A. Coddington, N. Levinson, *Theory of ordinary differential equations*, New York: McGraw–Hill, 1955.

21. J. K. Hale, *Ordinary differential equations*, New York: Dover Publications, 2009.

22. P. van den Driessche, J. Watmough, Reproduction numbers and sub-threshold endemic equilibria for compartmental models of disease transmission, *Math. Biosci.*, **180** (2002), 29–48. https://doi.org/10.1016/S0025-5564(02)00108-6

23. O. Diekmann, J. A. P. Heesterbeek, M. G. Roberts, The construction of next-generation matrices for compartmental epidemic models, *J. R. Soc. Interface*, **7** (2010), 873–885. https://doi.org/10.1098/rsif.2009.0386

24. J. K. Hale, P. Waltman, Persistence in infinite-dimensional systems, *SIAM J. Math. Anal.*, **20** (1989), 388–395. https://doi.org/10.1137/0520025

25. H. L. Smith, H. R. Thieme, *Dynamical systems and population persistence*, Graduate Studies in Mathematics, Vol. 118, Providence, RI: American Mathematical Society, 2011. https://doi.org/10.1090/gsm/118

26. X. Q. Zhao, *Dynamical systems in population biology*, New York: Springer, 2003. https://doi.org/10.1007/978-0-387-21761-1

27. H. I. Freedman, P. Waltman, Persistence in models of three interacting predator–prey populations, *Math. Biosci.*, **68** (1984), 213–231. https://doi.org/10.1016/0025-5564(84)90032-4

28. M. Y. Li, J. S. Muldowney, A geometric approach to global-stability problems, *SIAM J. Math. Anal.*, **27** (1996), 1070–1083. https://doi.org/10.1137/S0036141094266449

29. F. R. Gantmacher, *The theory of matrices*, Vol. 2, New York: Chelsea Publishing, 1959.

30. C. Castillo-Chavez, B. Song, Dynamical models of tuberculosis and their applications, *Math. Biosci. Eng.*, **1** (2004), 361–404. https://doi.org/10.3934/mbe.2004.1.361

31. W. H. Fleming, R. W. Rishel, *Deterministic and stochastic optimal control*, New York: Springer, 1975. https://doi.org/10.1007/978-1-4612-6380-7

32. L. S. Pontryagin, V. G. Boltyanskii, R. V. Gamkrelidze, E. F. Mishchenko, *The mathematical theory of optimal processes*, New York: Interscience Publishers, 1962.

33. S. Lenhart, J. T. Workman, *Optimal control applied to biological models*, Chapman & Hall/CRC, Boca Raton, FL, 2007. https://doi.org/10.1201/9781420011418

34. G. Zhang, Y. Shen, B. Chen, Positive periodic solutions in a non-selective harvesting predator–prey model with multiple delays, *J. Math. Anal. Appl.*, **395** (2012), 298–306. https://doi.org/10.1016/j.jmaa.2012.05.045

AIMS Press